Water Research 84 (2015) 1–10

Contents lists available at ScienceDirect

Water Research

journal homepage: www.elsevier.com/locate/watres

Inhibitory effect of natural organic matter or other background constituents on photocatalytic advanced oxidation processes: Mechanistic model development and validation

Jonathon Brame [a, 1, 2], Mingce Long [b, 2], Qilin Li [a], Pedro Alvarez [a, *]

[a] Rice University Department of Civil and Environmental Engineering, Houston, TX, USA
[b] Shanghai Jiao Tong University, School of Environmental Science and Engineering, Shanghai, China

ARTICLE INFO

Article history:
Received 22 April 2015
Received in revised form
24 July 2015
Accepted 26 July 2015
Available online 29 July 2015

Keywords:
Photocatalysis
TiO_2
Inhibitory model
Natural organic matter
Reactive oxygen

ABSTRACT

The ability of reactive oxygen species (ROS) to interact with priority pollutants is crucial for efficient water treatment by photocatalytic advanced oxidation processes (AOPs). However, background compounds in water such as natural organic matter (NOM) can significantly hinder targeted reactions and removal efficiency. This inhibition can be complex, interfering with degradation in solution and at the photocatalyst surface as well as hindering illumination efficiency and ROS production. We developed an analytical model to account for various inhibition mechanisms in catalytic AOPs, including competitive adsorption of inhibitors, scavenging of produced ROS at the surface and in solution, and the inner filtering of the excitation illumination, which combine to decrease ROS-mediated degradation. This model was validated with batch experiments using a variety of ROS producing systems (•OH-generating TiO_2 photocatalyst and H_2O_2-UV; $^1O_2$-generating photosensitive functionalized fullerenes and rose bengal) and inhibitory compounds (NOM, *tert*-butyl alcohol). Competitive adsorption by NOM and ROS scavenging were the most influential inhibitory mechanisms. Overall, this model enables accurate simulation of photocatalytic AOP performance when one or more inhibitory mechanisms are at work in a wide variety of application scenarios, and underscores the need to consider the effects of background constituents on degradation efficiency.

Published by Elsevier Ltd.

1. Introduction

Photochemical and photocatalytic processes offer unique capabilities to treat many common water pollutants as well as recalcitrant contaminants of emerging concern, including pharmaceutical products, endocrine disrupting compounds, and pesticides (Qu et al., 2012; Chong et al., 2010; Klavarioti et al., 2009; Brame et al., 2011). These advanced oxidation processes (AOPs) rely primarily on the strong oxidation potential of produced reactive oxygen species (ROS) such as hydroxyl radicals (•OH; 2.8 V vs. SHE (Klamerth et al., 2012)) or singlet oxygen ($^1O_2$, 1.1 V vs. SHE (Ahmad and Armstrong, 1984)). Photocatalysis offers a potentially cost-effective avenue for contaminant removal through extensive material reuse, use of solar illumination energy and utilization of existing UV disinfection infrastructure to achieve more efficient treatment.

Photocatalytic processes must account for and overcome various inhibition mechanisms in complex water matrices to enable implementation as a viable water treatment technology. For example, non-target organics can scavenge produced ROS, shade the photocatalytic materials from incoming photons (inner filter effect (Guillard et al., 2005)), and adsorb to the photocatalyst surface where they both displace adsorption of the target contaminants and potentially interfere with ROS production processes. We recently developed an analytical model to account for the inhibitory effect of background constituents such as dissolved organic matter and inorganic ions on the efficiency of homogeneous photoreactive AOP systems (Brame et al., 2014a). In this paper we expand this model to consider more common heterogeneous photocatalytic systems, in which additional inhibition mechanisms may interplay. Specifically, we consider ROS scavenging both in solution and at the photocatalyst surface, competition for surface adsorption

* Corresponding author.
E-mail address: alvarez@rice.edu (P. Alvarez).
[1] Present affiliation: US Army Engineer Research and Development Center, Vicksburg, MS, USA.
[2] Both these authors contributed equally to this work.

http://dx.doi.org/10.1016/j.watres.2015.07.044
0043-1354/Published by Elsevier Ltd.

sites between target contaminants and background materials, and light occlusion effects due to inner filtering.

To accurately predict AOP inhibition in natural waters, models must account for all of these processes—both surface and bulk phenomena—since inhibitory mechanisms are likely to affect not only bulk ROS concentration, but also surface concentrations and generation mechanisms. However, existing models of photocatalytic processes are limited by assumptions of either bulk degradation of contaminants by a steady state ROS concentration or surface degradation following adsorption of the contaminant to the photocatalyst surface (i.e., Langmuir–Hinshelwood kinetics, (Konstantinou and Albanis, 2004)). Herein we develop a model to account for both bulk and surface inhibition mechanisms simultaneously, allowing prediction of photocatalytic AOP inhibition due to non-target compounds present in treatment water, such as background natural organic matter (NOM). Validation of the model was carried out using several different combinations of photocatalysts, ROS probes and inhibitory compounds, to investigate the sensitivity of the model to variations in parameters such as adsorption capacity, ROS generation rate, type ($OH^{\bullet}$ and $^1O_2$) and scavenging potential.

2. Materials and methods

2.1. Photo-reactive testing

Both homogeneous and heterogeneous photoactive systems were used to validate the model and ensure its applicability to a wide variety of photo-active AOPs. Hydroxyl radical-producing materials used were titanium dioxide (TiO_2) as a heterogeneous system and UV-hydrogen peroxide (H_2O_2) as a homogeneous system. TiO_2 was Degussa P25 with a nominal particle size of 30 nm and surface area of 50 m^2/g (Jafry et al., 2010). H_2O_2 (35 wt%) was supplied by Fischer Scientific. Singlet oxygen-producing materials used were functionalized fullerenes (heterogeneous system) and rose bengal (RB; homogeneous system). The fullerene photocatalyst (Si–C_{60}) was an amine-functionalized C_{60} material covalently attached to a silica gel substrate by amide bonds. RB was supplied by Sigma–Aldrich. Photocatalyst loading (TiO_2, Si–C_{60}) was set at 0.5 g/L to simulate potential treatment conditions (Brame et al., 2013; Lee et al., 2010), and homogeneous photosensitizer concentrations (H_2O_2, RB) were chosen to match the steady state ROS production of the photocatalyst materials (15 mg/L, and 25 mg/L respectively). While other ROS species (e.g., super oxide) could be generated by photo-reactive materials, electron paramagnetic resonance (EPR) analysis showed that our systems primarily generate $^{\bullet}OH$ and $^1O_2$, respectively (Brame et al., 2014a, 2013; Lee et al., 2010; Liao et al., 2013).

All photocatalytic tests were conducted using a box photoreactor described extensively in previous works (Brame et al., 2013; Lee et al., 2010; Liao et al., 2013; Kim et al., 2012). Illumination was provided by six 4 W bulbs with UV-A (TiO_2, 350–400 nm), UV-C (H_2O_2, 254 nm) or visible (Si–C_{60}, RB; 400–800 nm) illumination spectra, with measured light intensities of 18 mW cm^{-2} (Brame et al., 2013), 165 mW cm^{-2} (Lee et al., 2010), and 1.105 mW cm^{-2} (Lee et al., 2011), respectively. Photo-reactive materials were stirred vigorously at room temperature in the 50 mL quartz reaction vessel with 1 mL sample aliquots taken at various time points for analysis. Probe compounds used as representative target pollutants included furfuryl alcohol (FFA, Sigma–Aldrich) and 4-chlorophenol (4CP, Sigma–Aldrich) (Brame et al., 2014a; Lee et al., 2010, Lee et al. 2009; Haag and Hoigne, 1986; Minero et al., 2000; Buxton et al., 1988; Brame et al., 2014b). These probe compounds were chosen due to their disparate properties (e.g., sorption, ROS reaction kinetics) to validate the model under a wide range of degradation circumstances. ROS ($OH^{\bullet}$ and $^1O_2$) production was confirmed previously using electron paramagnetic resonance (EPR) spectrometry, with typical values of 5.5×10^{-14} mg/L ($^{\bullet}OH$) and 5.64×10^{-13} mg/L ($^1O_2$) (Brame et al., 2014a).

2.2. Analysis

Quantification of FFA and 4CP concentration was carried out with a Shimadzu Prominence HPLC (Shimadzu Corp., Columbia MD) using a C18 column with acetonitrile and 0.1% (w/v) phosphoric acid as mobile phase solvents (70:30, FFA; 55:45, 4CP). Pseudo first order degradation rate constants (k_A) were estimated (±standard deviation) from a linear regression of observed exponential decay of compound concentrations as a function of time. To avoid influence of degradation byproducts, rate constants were calculated using only the early time data, representing the first 30% of degradation. All HPLC solvents were analytical-grade and obtained from Sigma–Aldrich.

2.3. Inhibitory compounds

Two different compounds were used to probe inhibitory mechanisms. Suwannee River NOM was used as a representative organic material, and was obtained from the International Humic Substances Society (St. Paul, MN, USA, (Hyung et al., 2006)). A second inhibitory compound, tert-butyl alcohol (t-BuOH), was used as a non-adsorbing comparison material, and was obtained from Sigma–Aldrich. Concentration ranges for inhibition compounds were chosen based on preliminary studies (data not shown) and previous findings (Brame et al., 2014a).

2.4. Kinetic model of ROS-mediated degradation

The initial ROS-mediated degradation of aqueous organic target compound A in water (prior to degradation product formation) can be modeled as a second order reaction:

$$\frac{dC_A}{dt} = k_A C_{ROS} C_A \quad (1)$$

Here C_A represents the concentration of the target compound being degraded (e.g., FFA), C_{ROS} represents the steady state ROS concentration in the system, and k_A is the reaction rate constant for a specific ROS compound reacting with target contaminant A in water. Literature values of k_A for a variety of compounds are available for both $^{\bullet}OH$ (Buxton et al., 1988) and $^1O_2$ (Wilkinson et al., 1995).

When degradation takes place on the photocatalyst surface, the same second order rate law is assumed with respect to the surface-bound concentrations of ROS and the target pollutant ($C_{ROS,S}$ and $C_{A,S}$, respectively). $C_{A,S}$ is a ratio of the occupied surface sites compared to the total number of surface sites, and is assumed to be in instantaneous equilibrium with the bulk aqueous phase concentration C_A, and is quantified using the Langmuir adsorption equilibrium model, which assumes a limited number of surface adsorption sites that can be filled to a monolayer of surface coverage in instantaneous equilibrium with the bulk concentration of the adsorbing compound (C_A):

$$C_{A,S} = q_A = \frac{K_A C_A}{1 + K_A C_A} \quad (2)$$

Where q_A is the equilibrium surface loading of A and K_A is the Langmuir adsorption constant. Inserting eq. (2) into eq. (1) yields an expression for ROS-mediated degradation at the surface of a

photocatalyst, the Langmuir–Hinshelwood (L–H) equation (El-Morsi et al., 2000; Enriquez and Pichat, 2001; Zhang et al., 1998):

$$\frac{dC_{A,S}}{dt} = \frac{k_A C_{ROS,S} K_A C_A}{1 + K_A C_A} \quad (3)$$

3. Results and discussion

3.1. Model development

To determine the overall inhibitory effect of non-target materials on photocatalytic degradation of a specific target compound, we adopt a mass-balance approach that accounts for ROS-mediated degradation in the bulk solution, adsorption interactions at the photocatalyst surface, and degradation by ROS and/or photo-generated holes at the photocatalyst surface. By examining these processes for both the target contaminants and inhibitory compounds, we can model interactions that inhibit degradation of the target material. Since surface concentration (q_A) and bulk concentration (C_A) are interdependent through equilibrium adsorption, degradation reactions both at the surface and in the bulk solution will influence contaminant concentrations and therefore reaction rates both at the surface and in solution. To express this interplay, we can describe the mass transport of compound A and ROS between the solution and the photocatalyst surface and degradation in the bulk solution and at the photocatalyst surface (Fig. 1).

The L–H equation (eq. (3)) is frequently used to describe surface photocatalytic reactions. Most other mechanistic photocatalytic reaction models developed from primary photocatalytic processes can be simplified to a similar form (Minero, 1999; Emeline et al., 2000), therefore the L–H equation was deemed suitable for the proposed model. Our model considers both surface and bulk reactions between the target contaminant and ROS (at steady state concentrations). The model assumes that the organic solute is adsorbed on the photocatalyst surface prior to reactions, while the bulk reaction rate is described by a second order bi-molecular reaction model. This model only requires bi-molecular reaction rate constants for the ROS-contaminant system, and the Langmuir adsorption isotherm parameters, which can all be determined independently without data fitting.

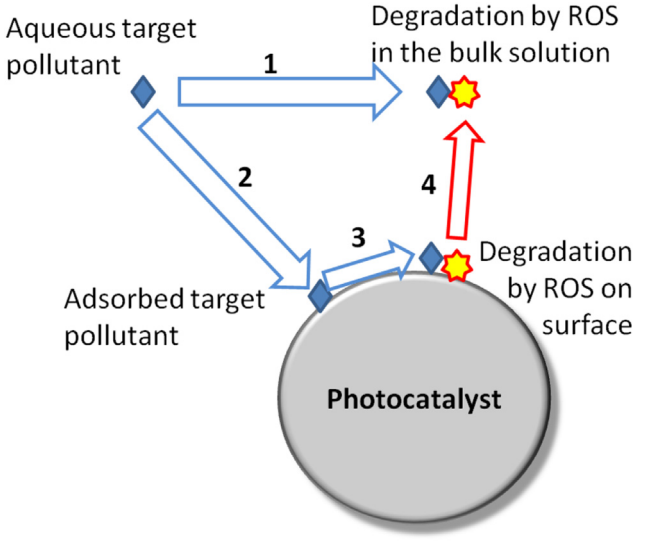

Fig. 1. Mass transport pathways during photocatalytic degradation. Pathway 1 represents bulk-phase degradation of the target compound by ROS. Pathway 2 represents reversible adsorption onto the photocatalyst surface. Pathway 3 represents degradation on the surface by ROS and photo-produced holes. Pathway 4 represents the transport of ROS from the photocatalyst surface into the bulk solution.

3.1.1. Assumptions

The model assumes that the inhibitory compound decreases the target compound degradation rate through three independent mechanisms: scavenging of ROS, competitive adsorption on photocatalyst surface and inner filtering of incident illumination. We also assume that adsorption equilibrium of both target and non-target compounds to photocatalyst surfaces can be described by the multi-solute Langmuir model (Turchi and Ollis, 1990), and that the Langmuir adsorption constant K_A is independent of irradiation. Next, it is assumed that the concentration of ROS at the photocatalyst surface and in the bulk ($C_{ROS,S}$ and $C_{ROS,B}$, respectively) are at steady state. This is a common assumption due to the short lifetime of ROS in aqueous solutions and the lack of ROS buildup observed in photocatalytic systems (Wilkinson et al., 1995; Tachikawa and Majima, 2009). $C_{ROS,S}$ in our model is assumed to include all oxidation species active at the surface of the photocatalyst, including photo-generated holes and surface-bound ROS. This simplification allows use of a single term for ROS generation and for ROS –mediated degradation kinetics regardless of the specific ROS species responsible for the degradation reaction.

We also assume a bi-molecular, second order reaction between ROS and the compound being oxidized (FFA, NOM, etc.), so one ROS molecule is consumed for every molecule that is oxidized. Since oxidation of reaction byproducts can further decrease the ROS concentration, the model is limited to initial degradation rates (first 20 min, generally) before significant byproduct formation. Lastly we assume an average ROS diffusion distance based on ROS diffusion coefficients (Tachikawa and Majima, 2009) to determine the ROS concentration gradient for Fickian diffusion. The diffusion coefficients used were for ROS compounds in water, but could be modified to include the effect of target and inhibitory compounds for increased accuracy.

Note that this model does not consider non-photocatalytic degradation processes such as photolysis or direct photo-oxidation. In many cases (including the validation studies presented), the pollutants targeted for photocatalytic degradation are sufficiently recalcitrant to preclude these peripheral photo-degradation processes, which should be confirmed using control experiments without photocatalyst (Figure S1, SI).

3.1.2. Degradation without inhibitory compounds

A mass balance for compound A in a photocatalytic system with no inhibitory compounds reveals that there are two sinks: degradation in the bulk aqueous phase (eq. (1)) and at the surface (eq. (3)) (Fig. 1, pathways 1 and 3, respectively).

$$\frac{dC_A}{dt} = -k_A C_{ROS,B} C_A - \frac{k_A C_{ROS,S} K_A C_A}{1 + K_A C_A}$$
$$= -k_A C_A \left(C_{ROS,B} + \frac{C_{ROS,S} K_A}{1 + K_A C_A} \right) \quad (4)$$

Since the ROS concentration at the surface and in the bulk aqueous phase are different, we denote them as $C_{ROS,S}$ and $C_{ROS,B}$, respectively. We can also perform a mass balance on ROS in the system, which is assumed to be at steady state. Production of ROS (P_{ROS}) takes place at the photocatalyst surface, and ROS is consumed in reactions with A either in solution or at the surface, while transport of ROS between the photocatalyst surface and solution is a diffusion flux (J_{ROS}, area normalized) (Fig. 1, pathways 1, 3 and 4, respectively):

$$\frac{dC_{ROS,B}}{dt} = J_{ROS} - k_A C_{ROS,B} C_A = 0 \quad (5)$$

$$\frac{dC_{ROS,S}}{dt} = P_{ROS} - J_{ROS} - \frac{k_A C_{ROS,S} K_A C_A}{1 + K_A C_A} = 0 \quad (6)$$

Since there is no accumulation or depletion of ROS in solution ($\frac{dC_{ROS,B}}{dt} = 0$), the transport of ROS (J_{ROS}) from the surface into the bulk is equal to the bulk degradation term in eq. (5), which can then be substituted into eq. (6) to solve for P_{ROS}:

$$P_{ROS} = -k_A C_{ROS,B} C_A - \frac{k_A C_{ROS,S} K_A C_A}{1 + K_A C_A} \quad (7)$$

The ROS concentration at the surface and in the bulk are related by Fick's first law, $J_{ROS} = D'^{*}\Delta C_{ROS}$ (D' is the diffusion coefficient [D] (Buxton et al., 1988; Tachikawa and Majima, 2009) normalized per unit diffusion length), which enables eq. (4) to be restated in terms of only the surface ROS concentration.

$$J_{ROS} = D'(C_{ROS,S} - C_{ROS,B}) \quad (8)$$

$$C_{ROS,S} = C_{ROS,B} + \frac{J_{ROS}}{D'} = C_{ROS,B} + \frac{k_A C_{ROS,B} C_A}{D'} = C_{ROS,B}\left(1 + \frac{k_A C_A}{D'}\right) \quad (9a)$$

$$C_{ROS,B} = \frac{C_{ROS,S}}{1 + \frac{k_A C_A}{D'}} \quad (9b)$$

$$\frac{dC_A}{dt} = -k_A C_A C_{ROS,S}\left(\frac{1}{1 + \frac{k_A C_A}{D'}} + \frac{K_A}{1 + K_A C_A}\right) \quad (10)$$

Eq. (10) incorporates the L–H equation to describe the photocatalytic degradation rate for a single probe compound accounting for degradation both at the surface and in solution. In cases where adsorption is negligible ($K_A << 1$), eq. (10) reduces to eq. (1), with C_{ROS} replaced according to eq. (9b). When bulk degradation is small ($\frac{k_A C_A}{D'} \gg 1$), eq. (10) reduces to eq. (3), which is the L–H model for surface-mediated degradation. $C_{ROS,S}$ and/or $C_{ROS,B}$ for a given photocatalyst material and treatment scenario can be determined experimentally for a given photocatalytic system using simple probe compounds (Brame et al., 2014a).

3.1.3. Degradation in the presence of inhibitory compounds

When an inhibitory compound such as NOM is present, there is competition for ROS in solution and at the surface, and for adsorption sites on the photocatalyst surface. Although NOM is a very complex combination of humic acids and other organic materials, we model it is a simple molecule for purposes of sorption and reaction interactions. For competitive adsorption, degradation follows a simple, multi-solute Langmuir equilibrium model (Abdullah et al., 1990):

$$\frac{dC_A}{dt} = \frac{k_A C_{ROS,S} K_A C_A}{1 + K_A C_A + K_N C_N} \quad (11)$$

The system mass balance on compound A then becomes

$$\frac{dC_A}{dt} = -k_A C_{ROS,B} C_A - \frac{k_A C_{ROS,S} K_A C_A}{1 + K_A C_A + K_N C_N} = -k_A C_A\left(C_{ROS,B} + \frac{C_{ROS,S} K_A}{1 + K_A C_A + K_N C_N}\right) \quad (12)$$

K_N is the Langmuir adsorption constant for the inhibition compound (N) adsorbing onto the photocatalyst surface and C_N is the equilibrium concentration of compound N in solution.

The mass balance on ROS in the system is adjusted to account for scavenging of ROS by the inhibitory compound both in bulk and at the surface. These reactions are identical to eqs. (1) and (3) with the subscript A replaced by N. Following the same derivation as for eqs. (8)–(10), we can determine the steady state production of ROS in the system:

$$\begin{aligned} P_{ROS} &= k_A C_{ROS,B} C_A + k_N C_{ROS,B} C_N + \frac{k_A C_{ROS,S} K_A C_A}{1 + K_A C_A + K_N C_N} \\ &\quad + \frac{k_N C_{ROS,S} K_N C_N}{1 + K_A C_A + K_N C_N} \\ &= k_A C_A\left(C_{ROS,B} + \frac{C_{ROS,S} K_A}{1 + K_A C_A + K_N C_N}\right) \\ &\quad + k_N C_N\left(C_{ROS,B} + \frac{C_{ROS,S} K_N}{1 + K_A C_A + K_N C_N}\right) \\ &= C_{ROS,B}(k_A C_A + k_N C_N) \\ &\quad + \frac{C_{ROS,S}}{1 + K_A C_A + K_N C_N}(k_A C_A K_A + k_N C_N K_N) \end{aligned} \quad (13)$$

We can again use eq. (8) to relate $C_{ROS,B}$ to $C_{ROS,S}$; however, in this case J_{ROS} at steady state is equal to the sum of bulk degradation of both A and N (adding the degradation of compound N to eq. (5)).

$$C_{ROS,S} = C_{ROS,B} + \frac{J_{ROS}}{D'} = C_{ROS,B} + \frac{k_A C_{ROS,B} C_A + k_N C_{ROS,B} C_N}{D'} = C_{ROS,B}\left(1 + \frac{k_A C_A + k_N C_N}{D'}\right) \quad (14a)$$

$$C_{ROS,B} = \frac{C_{ROS,S}}{1 + \frac{k_A C_A + k_N C_N}{D'}} \quad (14b)$$

Inserting eq. (14b) into eq. (13) yields:

$$\begin{aligned} P_{ROS} &= \frac{C_{ROS,S}}{1 + \frac{k_A C_A + k_N C_N}{D'}}(k_A C_A + k_N C_N) \\ &\quad + \frac{C_{ROS,S}}{1 + K_A C_A + K_N C_N}(k_A C_A K_A + k_N C_N K_N) \\ &= C_{ROS,S}\left[\frac{1}{1 + \frac{k_A C_A + k_N C_N}{D'}}(k_A C_A + k_N C_N)\right. \\ &\quad \left. + \frac{1}{1 + K_A C_A + K_N C_N}(k_A C_A K_A + k_N C_N K_N)\right] \end{aligned} \quad (15)$$

$$C_{ROS,S} = \frac{P_{ROS}}{\frac{1}{1 + \frac{k_A C_A + k_N C_N}{D'}}(k_A C_A + k_N C_N) + \frac{1}{1 + K_A C_A + K_N C_N}(k_A C_A K_A + k_N C_N K_N)} \quad (16)$$

Combining eqs. (14b) and (16) back into eq. (12) and simplifying

yields an expression for overall degradation rate of the target compound (A) in terms of the ROS production rate and concentration of inhibitory compound.

$$\frac{dC_A}{dt} = \frac{-P_{ROS}}{1 + \frac{k_N C_N (F + K_N S)}{k_A C_A (F + K_A S)}} \quad (17)$$

Where $F = \frac{1}{1 + \frac{k_A C_A + k_N C_N}{D'}}$; $S = \frac{1}{1 + K_A C_A + K_N C_N}$

Equation (17) is a general expression for steady state ROS-mediated photocatalytic degradation of compound A in the presence of NOM or any other ROS-scavenging material.

3.1.4. Light absorption

In addition to the changes in degradation discussed above, the addition of inhibitory compounds can also alter the ROS production rate (P_{ROS}) by absorbing light, thus reducing illumination available for ROS production. This inner filter effect due to light attenuation can be accounted for using the Beer–Lambert law, in which P_{ROS} will be attenuated by the factor $10^{-\mu\ell C_N}$, where μ is the specific absorption coefficient of the material and ℓ is the optical path length of the incoming light (Brame et al., 2014a; Bezares-Cruz et al., 2004).

$$\frac{P_{ROS}}{P_{ROS,0}} = 10^{-\mu\ell C_N} \quad (18)$$

The subscript 0 on P_{ROS} indicates the ROS production rate without light attenuation. Plugging the modified ROS production rate into eq. (17) we can model the total decrease in degradation due to scavenging, competitive adsorption and light attenuation.

$$\frac{dC_A}{dt} = \frac{-P_{ROS,0}}{1 + \frac{k_N C_N (F + K_N S)}{k_A C_A (F + K_A S)}} 10^{-\mu\ell C_N} \quad (19)$$

Since μ is a function of wavelength for each inhibitory material and ℓ is a function of reactor geometry, the combined factor $\mu\ell$ can be obtained by numerically integrating absorbance and illumination path-length over the relevant wavelength range and reactor geometry, as shown previously (Brame et al., 2014a; Bezares-Cruz et al., 2004).

3.2. Model validation

To validate this model we used a variety of photocatalytic materials, probe compounds and inhibition compounds to survey the effect of various adsorption and kinetic properties between the reacting materials. We then compared the measured degradation rates in these conditions to the degradation rates predicted by the model developed above. Photocatalytic materials tested included Degussa P25 TiO_2, which produces primarily •OH, and amino-functionalized fullerenes attached to a silica gel substrate, which produce primarily $^1O_2$. For further validation, we also evaluated the proposed model using data from previously published homogeneous photo-reactive systems (UV/H_2O_2 and rose bengal (Brame et al., 2014a)) to ensure that this more general model is capable of predicting inhibition in a wide variety of AOP systems. Calibration of the model was accomplished by measuring the production of ROS in the absence of inhibition compounds (P_{ROS}), which provides a baseline for comparison as C_N increases. Note that since the model predicts relative degradation rates (normalized to degradation in absence of inhibitory compounds), the P_{ROS} term cancels, enabling the model to be validated independently.

Modeling parameters are given in Table 1. Degradation rate constants (k_A, k_N) and diffusion constants (D) were taken from reviews in the Journal of Physical and Chemical Reference Data providing kinetic parameters for myriad chemical compounds reacting with •OH (Buxton et al., 1988) and $^1O_2$ (Wilkinson et al., 1995). When rate constant values were not available from literature sources, they were estimated using EPI Suite, or measured independently using a known ROS concentration in ultrapure water (Brame et al., 2014a). Sorption parameters (K_A, K_N) were measured for this study using Langmuir adsorption isotherms, or taken from literature sources using identical photocatalytic materials (Martínez et al., 2011). Finally, the inner filter constant was calculated by measuring the absorbance of the NOM at each wavelength according to the Beer–Lambert law, following the method derived previously for homogeneous photoreactions (Brame et al., 2014a).

Validation compounds were chosen with wide variation in these parameters to show the flexibility of the model. For example, one of the probe compounds used (4CP) significantly adsorbs to the photocatalyst materials, while the other (FFA) does not ($K_A << 1$); and, since •OH are much more easily scavenged by NOM than $^1O_2$, •OH -based degradation reactions are more inhibited than $^1O_2$ reactions in the presence of NOM (k_N for $^1O_2 \approx 0$) (Brame et al., 2014a). Similarly, the inhibitory compounds provide further differentiation. NOM absorbs light strongly in both the visible and UV spectrum and adsorbs to photocatalysts' surfaces, while t-BuOH neither absorbs light ($\mu\ell << 1$) or adsorbs to the photocatalyst ($K_N << 1$). Figs. 2–4 show the ability of the model to predict degradation rates for these various photocatalytic treatment parameters including treatment with TiO_2 (Fig. 2), Si–C_{60} (Fig. 3) and homogeneous photo-sensitizers RB and H_2O_2 (Fig. 4). In all cases tested, the model predicts the degradation rates with a high degree of accuracy ($r^2 > 0.88$, $p < 0.05$). These results validate the proposed model, and show its capability to predict degradation for a wide variety of possible photocatalytic water treatment scenarios.

3.3. Sensitivity analysis

A sensitivity analysis was performed to discern the most influential variables and determine which coefficients are most susceptible to compounding error within the model. Parameter values from eq. (19) (Table 1) were varied by ±50% using a one-factor-at-a-time (OAT) method (Saltelli et al., 2005) to compare the point elasticity of the predicted degradation rate (dC_A/dt). Point elasticity is a measure of how sensitive the system is to a given parameter and it is defined as the percent change in the dependent variable (in this case degradation rate) divided by the percent change in an independent variable (Gomez et al., 2008). A point elasticity value of 1 for a given parameter indicates that a 10% change in that parameter will result in a 10% change in the modeled degradation rate. Table 2 shows the individual point elasticity values for the parameters from eq. (19) for each of the photo-reactive systems described in Figs. 2–4. Some of the parameters in these individual cases have no point elasticity because their values are small/zero. To account for this, we have also calculated the average point elasticity (Table 3), using parameter values depicted in Table 1.

The most sensitive parameter was the photocatalyst ROS production rate ($P_{ROS,0}$). The elasticity value of 1 is intuitive from eq. (19), where $P_{ROS,0}$ is directly proportional to the modeled degradation rate. $P_{ROS,0}$ is effectively a scaling factor describing the ability of the photo-reactive material to generate ROS, and the amount of ROS produced affects degradation through each of the pathways described in sections 3.2–3.3. Analysis of other sensitive parameters, including degradation rate constants, inner filter coefficients, and adsorption constants, yields insight into the relative importance of the mechanisms considered by the model.

The inhibitory compound reaction rate constant (k_N) and sorption constant (K_N) were the next most sensitive parameters with

Table 1
Parameters used in this model.

Photo-material	TiO_2				$Si-C_{60}$	H_2O_2	RB	TiO_2			
ROS type	$OH^•$				$^1O_2$	$OH^•$	$^1O_2$	$^•OH$			
Probe compound (A)	FFA		4CP		FFA	FFA	FFA	Diclofenac		17α-ethynylestradiol	
Inhibitory compound (N)	NOM	t-BuOH	NOM	t-BuOH	NOM	NOM	NOM	NOM	t-BuOH	NOM	t-BuOH
Reaction rate constant (A) (k_A, L/g s^{-1})	[a]1.5×10^8		[a]5.9×10^7		[b]1.2×10^6	[a]1.5×10^8	[b]1.2×10^6	[c]3.4×10^8	[c]3.4×10^8	[c]2.5×10^8	[c]2.5×10^8
Reaction rate constant (N) (k_N, L/g s^{-1})	[d]1.3×10^4	[b]7.7×10^5	[d]1.3×10^4	[b]7.7×10^5	NM	[d]1.3×10^4	NM	[d]1.3×10^4	[b]7.7×10^5	[d]1.3×10^4	[b]7.7×10^5
Langmuir adsorption constant (K_A, L/mg)	NM		[d]8.8×10^4		NM	NM	NM	[e]8.8×10^4	[e]8.8×10^4	[f]NM	[f]NM
Langmuir adsorption constant (K_N, L/mg)	[d]1.1×10^5	NM	[d]1.1×10^5	NM	[d]8.8×10^3	NM	NM	[d]1.1×10^5	NM	[d]1.1×10^5	NM
Diffusion coefficient (D, m^2 s^{-1})	[a]0.17				[g]0.15	N/A	N/A	[a]0.17	[a]0.17	[a]0.17	[a]0.17
Inner filter constant (μℓ, L/mg)	[d]14×10^{-3}	NM	[d]14×10^{-3}	NM	[d]5.7×10^{-3}	[h]20×10^{-3}	[h]11×10^{-3}	[d]14×10^{-3}	NM	[d]14×10^{-3}	NM

NM = Not Measureable, ≈0.
[a] (Buxton et al., 1988).
[b] (Wilkinson et al., 1995).
[c] EPI Suite.
[d] This study.
[e] (Martínez et al., 2011).
[f] (Frontistis et al., 2012).
[g] (Skovsen et al., 2005).
[h] (Brame et al., 2014a).

average point elasticity values of 0.96 (Table 3) and several individual point elasticity values >0.84 (Table 2). The large elasticity of parameters relating to the inhibition compound is indicative of the importance of ROS scavenging and competitive sorption in photocatalytic processes, confirming that the presence of background organics could have significant effects on the efficiency of AOP systems.

The inner filter effect (average point elasticity: 0.51) is another parameter not often accounted for in photocatalytic studies, but which could significantly decrease the efficiency of photocatalytic AOPs (Brame et al., 2014a). For example, individual point elasticity values >0.80 (Table 2) show the strong influence of NOM on UV-TiO_2 systems. Background materials that absorb light could seriously impede illumination within a reactor system, and thereby

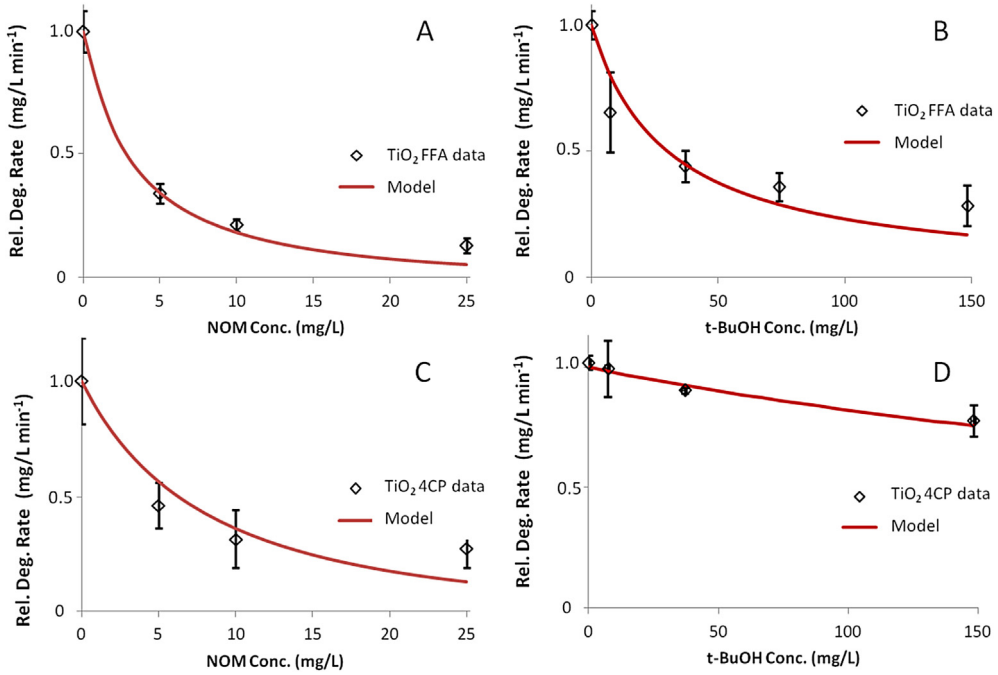

Fig. 2. Measured and modeled relative degradation rates (degradation rate divided by rate without inhibitor) as a function of inhibitor concentration for the degradation of FFA (A and B) and 4CP (C and D) by TiO_2 photocatalyst producing $OH^•$. The model (eq. (19)) fits the data with an r^2 value of 0.98 (A), 0.88 (B), 0.91 (C) and 0.96 (D) ($p < 0.05$). $[FFA]_0 = 25$ mg/L, $[4CP]_0 = 2.5$ mg/L, $[TiO_2]_0 = 0.5$ g/L.

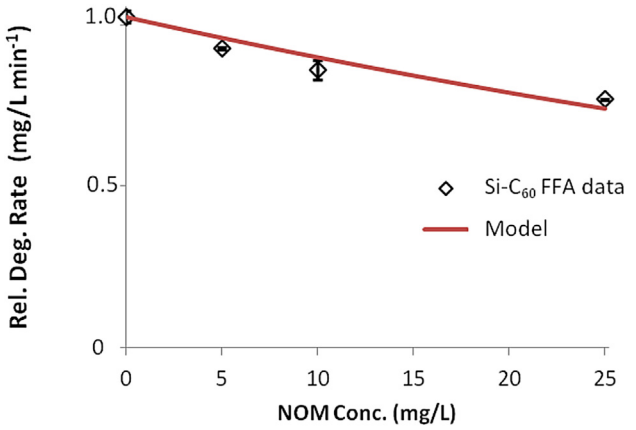

Fig. 3. Measured and modeled relative degradation rate (degradation rate divided by rate without inhibitor) as a function of NOM concentration for the degradation of FFA by Si–C_{60} photocatalyst producing $^1O_2$. The model (eq. (19)) fits the data with an r^2 value of 0.90 ($p < 0.05$). $[FFA]_0 = 25$ mg/L, $[Si–C_{60}]_0 = 0.5$ g/L.

limit treatment effectiveness. However in some cases—such as t-BuOH with UV light (point elasticity = 0, Table 2)—inner filtering has no effect because the wavelength of light absorbed by the inhibitory compound does not align with the excitation wavelength of the photocatalyst. A more complete understanding of inhibition mechanisms provided by this model could, for example, help inform an AOP user if pre-treatment to remove background, light-attenuating compounds would markedly improve degradation kinetics. This highlights the significance of identifying, understanding and characterizing the inhibition mechanisms likely to occur in a photo-reactive system to overcome potential efficiency barriers.

3.4. Mechanistic insights

The proposed model allows insight into the relative importance of multiple inhibitory mechanisms, and can be used to help inform process and photocatalyst design for photo-reactive systems. For example, this model can enable quantitative prediction of inhibition processes that have previously been only described qualitatively, such as inhibition of degradation of persistent organic pollutants in the presence of NOM (Lee et al., 2011; Doll and Frimmel, 2005a; Zhang et al., 2014) or in wastewater treatment (Lee and von Gunten, 2010; Doll and Frimmel, 2005b; Arslan et al., 2000). These inhibitory effects depend significantly on the properties of the target compound, the inhibitory compounds and the

Table 2
Point elasticity of target compound degradation rates (dC_A/dt, eq. (19)) for each parameter for the cases discussed in Figs. 2–4.

Photo-active material	TiO_2				Si–C_{60}	H_2O_2	RB
Probe compound	FFA		4CP		FFA	FFA	FFA
Inhibitory compound	NOM	t-BuOH	NOM	t-BuOH	NOM	NOM	NOM
k_A	0.88	0.27	0.76	0.83	0.00	0.12	0.00
k_N	3.11	0.24	0.84	1.00	0.00	0.12	0.00
$P_{ROS,0}$	1.00	1.00	1.00	1.00	1.00	1.00	1.00
K_A	0.00	0.00	0.76	0.83	0.00	0.00	0.00
K_N	0.00	0.00	0.84	1.00	0.00	0.00	0.00
D′	0.00	0.00	0.00	0.00	0.00	0.00	0.00
μl	0.82	0.00	0.80	0.00	0.32	0.54	0.29

Table 3
Average point elasticity of parameters with respect to target compound degradation rates (dC_A/dt, eq. (19)), determined using characteristic parameter values from Table 1.

Parameter	Parameter value	Average point elasticity
k_A	1.5×10^8 L/g s^{-1}	0.81
k_N	1.3×10^4 L/g s^{-1}	0.96
$P_{ROS,0}$	0.2 min^{-1}	1.00
K_A	8.8×10^4 L/mg	0.81
K_N	1.1×10^5 L/mg	0.96
D′	0.15 L/mg	0.00
μl	10×10^{-3} L/mg	0.51

ROS-generating photoactive materials, as reflected by the modeling parameters (Table 1). A comparison of •OH -generating and $^1O_2$-generating photo-reactive processes shows that NOM exerts a greater inhibitory effect in •OH -mediated systems than in those that produce $^1O_2$. Figs. 2A, B, C and 4B—all of which are •OH -producing systems—each show a >75% decrease in degradation rate in the presence of background materials (25 mg/L NOM, 150 mg/L t-BuOH), while degradation rates in $^1O_2$-producing systems decreased by less than 15% (Figs. 3 and 4A). This is consistent with previous findings that show singlet oxygen to be a much more selective oxidant, and therefore much less susceptible to scavenging by non-target contaminants such as NOM (Brame et al., 2014a).

Although the inhibitor t-BuOH has a much higher reaction rate constant than NOM (7.7×10^5 vs 1.3×10^4 L/g s^{-1}), the higher adsorption affinity of NOM onto the TiO_2 surface makes NOM a stronger inhibitor (Fig. 2A, C vs. 2B, 2D). However, target substrates with higher adsorption propensity (e.g., 4CP) can counteract

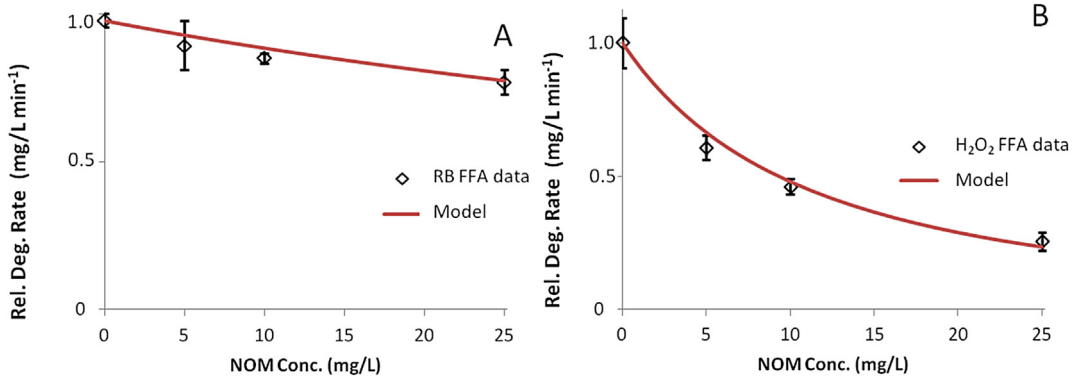

Fig. 4. Measured and modeled relative degradation rates (degradation rate divided by rate without inhibitor) as a function of NOM concentration for the degradation of FFA by RB (A) and H_2O_2 (B). The model (eq. (19)) fits the data with an r^2 value of 0.90 (A) and 0.97 (B) ($p < 0.05$). $[FFA]_0 = 25$ mg/L, $[H_2O_2]_0 = 15$ mg/L, $[RB]_0 = 25$ mg/L. Modified from Brame et al. (2014a).

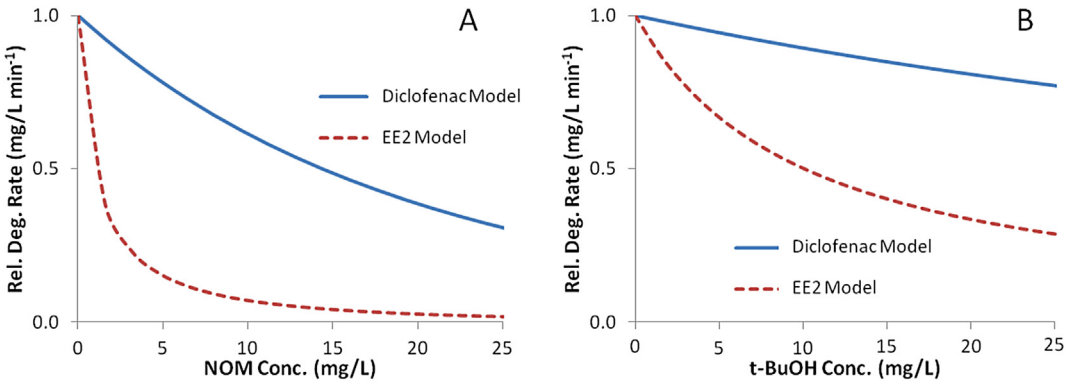

Fig. 5. Degradation rates as a function of inhibitor compound (NOM-A; t-BuOH-B) predicted by the model (eq. (19)) for two emerging contaminants, diclofenac and 17α-ethynylestradiol (EE2).

inhibition by NOM to a certain extent through competitive adsorption. Fig. 2D is an important case of this mechanism, wherein the strong adsorption of 4CP to the TiO_2 surface substantially counteracts the strong ROS scavenging of a •OH –mediated system.

Overall, these results show the ability of the model to accurately predict photocatalytic AOP performance for a wide variety of possible implementation scenarios, which is important to support the design and operation of robust treatment systems. For example, Fig. 5 shows model simulations for the photocatalytic degradation of two pollutants of emerging concern, diclofenac and 17α-ethynylestradiol (EE2). Sorption constants onto TiO_2 were obtained from the literature, while •OH degradation rate constants were estimated from structure–activity relationships using EPI Suite (Table 1). These two compounds provide an interesting theoretical comparison because they have similar degradation kinetics, but different sorption properties ($K_{A,diclofenac} >> K_{A,EE2}$). In the presence of a strongly adsorbing inhibitor (NOM), predicted EE2 degradation falls off dramatically, while predicted diclofenac degradation

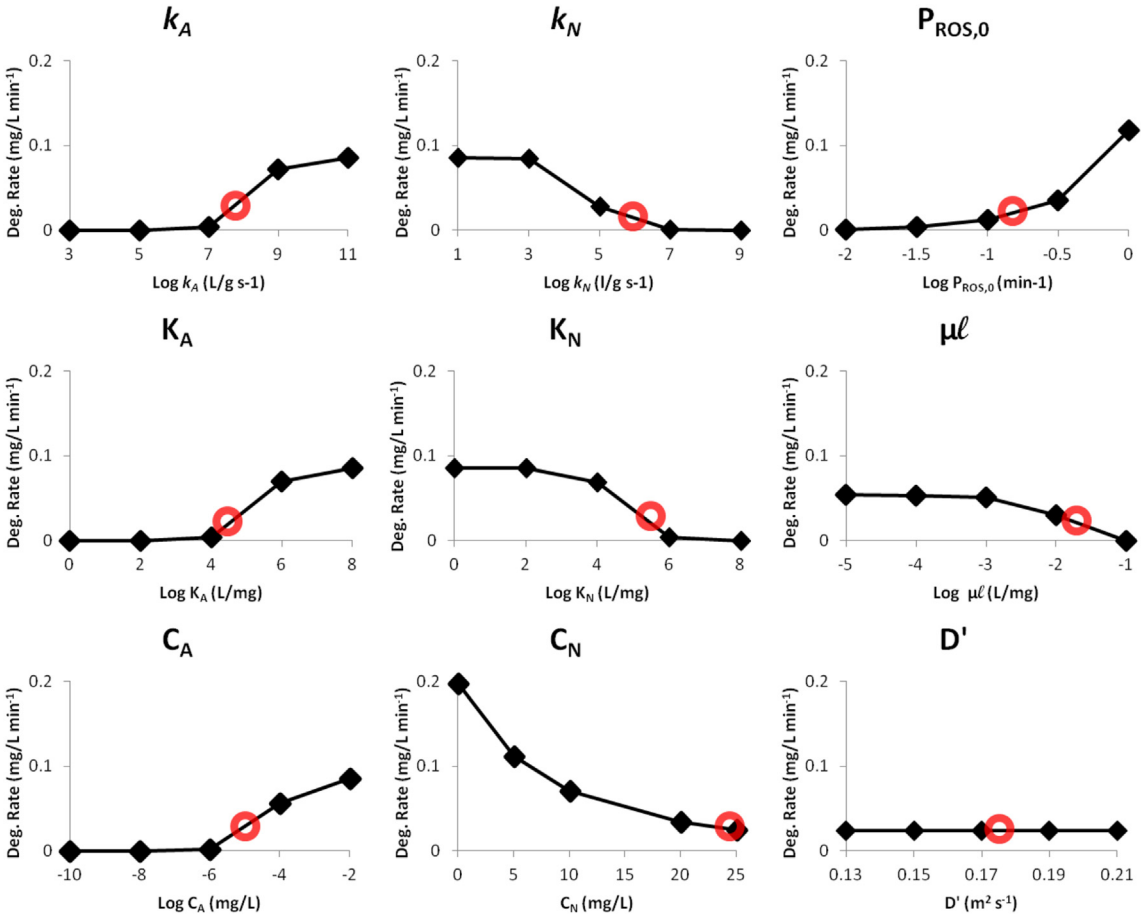

Fig. 6. Influence of each model parameter on degradation rate (eq. (19)) with all other parameters held constant. The variation scale of each parameter (x-axis) was chosen to extend beyond extreme high and low values for that parameter reported in the literature. The red circles indicate the value of that parameter held constant in each of the other graphs (For interpretation of the references to color in this figure legend, the reader is referred to the web version of this article.).

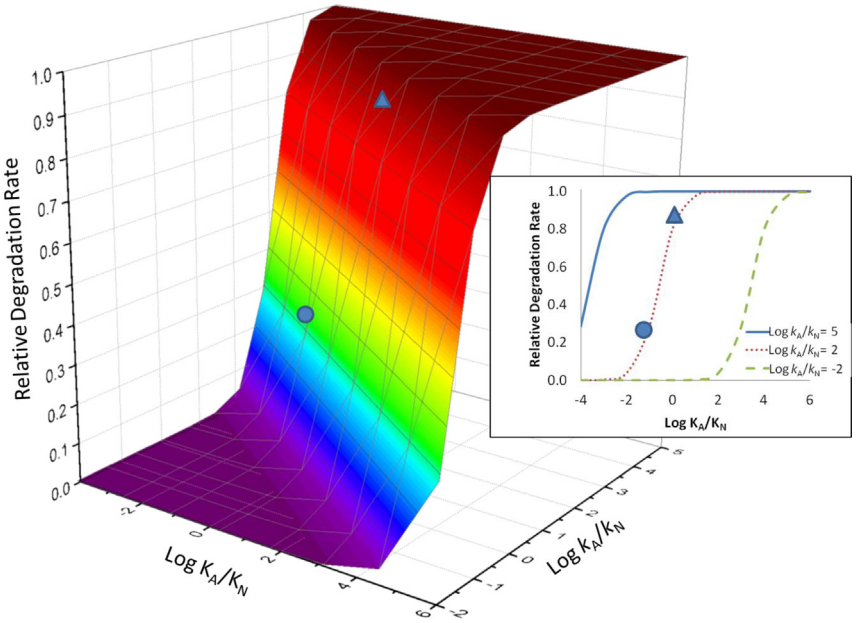

Fig. 7. Influence of competitive adsorption (K_A/K_N) and ROS scavenging (k_A/k_N) inhibition mechanisms on degradation efficiency according to the model (eq. (19)). Relative degradation rate represents the ratio of the degradation rate in the presence/absence of background materials. Inset shows several slices of the 3-dimensional graph with ROS scavenging representative of a $^1O_2$ system (Log $k_A/k_N = 5$), a •OH -producing system (Log $k_A/k_N = 2$) and a system with extreme scavenging (Log $k_A/k_N = -2$). The triangle and circle on the graphs indicate dicloferan and EE2, respectively, in the presence of t-BuOH (Log $k_A/k_N \approx 2$; Log $K_A/K_N = -0.5$ (dicloferan), -2 (EE2); see Fig. 5).

decreases much more slowly because it is able to compete with NOM for adsorption sites on the TiO_2 surface. Both compounds should be less inhibited by t-BuOH, which does not adsorb strongly to TiO_2. In this case, the simulated degradation of diclofenac is only slightly inhibited because the majority of degradation takes place at the photocatalyst surface, while the model predicts EE2 degradation to be moderately inhibited due to scavenging of •OH by t-BuOH.

Understanding the influence of each of the model parameters on degradation efficiency can also help inform system requirements to overcome potential losses of efficiency due to inhibition. Fig. 6 shows the relative influence of each model parameter on overall degradation efficiency when all other parameters are held constant. Increasing values of k_A, K_A, C_A and $P_{ROS,0}$ results in increased degradation rate, as adsorption of the target pollutant, ROS generation and degradation kinetics are increased. Meanwhile increasing values of k_N, K_N, C_N and μl correspond to a larger influence of the inhibitory compound and therefore more inhibition (decreasing degradation rates).

In some cases, it is not the absolute value of a parameter, but the parameter's value in relation to another parameter that influences inhibition in the system. Of special interest is the ratio of the adsorption constants of A and N (K_A/K_N), which indicates the influence of competitive adsorption, and the ratio of the degradation rate constants of A and N (k_A/k_N), which indicates the influence of ROS scavenging in the system. Fig. 7 shows a 3-dimensional plot of the relative degradation rate (ratio of the degradation rate in the presence/absence of background materials) as a function of both the competitive adsorption (K_A/K_N) and ROS scavenging (k_A/k_N) in a photocatalytic system. The regions of especially high and low inhibitory effect are intuitive, corresponding to high and low competitive adsorption and scavenging, respectively. However, the shape of the graph indicates that to some extent, the presence of significant inhibition by either mechanism can be overcome by engineering a system to minimize the effect of the other. For example, a system with significant inefficiency due to competitive adsorption can avoid inhibition by using a photocatalytic process that is highly selective, such as a $^1O_2$-generating process. The two emerging contaminants modeled in Fig. 5B are represented as a triangle mark (diclofenac) and circle (EE2) on the graphs in Fig. 7. Both of these compounds have similar scavenging potential (Log $k_A/k_N \approx 2$), but diclofenac is much less prone to competitive sorption inhibition than EE2 due to its higher adsorption capacity (Log $K_A/K_N = -0.5, -2$ respectively). By tracing these parameters on the 3D graph of Fig. 7, we can estimate the degradation efficiency modeled in Fig. 5B.

The inset chart in Fig. 7 shows several slices of the 3-dimensional graph with k_A/k_N values representing $^1O_2$ ($k_A/k_N = 10^5$), •OH ($k_A/k_N = 10^2$) and a case of extreme scavenging ($k_A/k_N = 10^{-2}$). For a $^1O_2$-mediated process, the influence of competitive adsorption is minimal, with no inhibition across several orders of magnitude of K_A/K_N, including negative log values, which represent cases where sorption of the non-target material dominates sorption of the target compound. Meanwhile, for •OH systems the adsorption constants must be at least comparable to avoid significant inhibition. In the case of excessive scavenging (e.g., a very difficult to degrade target compound with a small k_A/k_N), only selective adsorption of the target compound can enable degradation without significant inhibition. This suggests that even very recalcitrant contaminants could be preferentially degraded in a system engineered to selectively adsorb the target compound (e.g., functionalized substrates for compound-specific adsorption). Further work is needed to explore this possibility.

4. Conclusion

This study reaffirms the importance of accounting for background NOM or other inhibitors during advanced oxidation, as degradation rates can decrease by one order of magnitude or more in the presence of such background water constituents. Our validated mechanistic model enables determination of these effects for ROS-mediated advanced oxidation processes in a wide variety of

implementation scenarios and source water characteristics. The model points to competitive adsorption by NOM and ROS scavenging as the most influential inhibitory mechanisms. By providing a novel analytical approach to simultaneously consider surface and solution photocatalytic oxidation, this model can help inform strategies to enhance the performance of AOPs, even in systems with high levels of NOM or other background constituents.

Appendix A. Supplementary data

Supplementary data related to this article can be found at http://dx.doi.org/10.1016/j.watres.2015.07.044.

References

Abdullah, M., Low, G.K.C., Matthews, R.W., 1990. Effects of common inorganic anions on rates of photocatalytic oxidation of organic carbon over illuminated titanium dioxide. J. Phys. Chem. 94 (17), 6820–6825.

Ahmad, R., Armstrong, D.A., 1984. The effect of pH and complexation on redox reactions between RS• radicals and flavins. Can. J. Chem. 62 (1), 171–177.

Arslan, I., Balcioglu, I.A., Bahnemann, D.W., 2000. Heterogeneous photocatalytic treatment of simulated dyehouse effluents using novel TiO(2)-photocatalysts. Appl. Catal. B Environ. 26 (3), 193–206.

Bezares-Cruz, J., Jafvert, C.T., Hua, I., 2004. Solar photodecomposition of decabromodiphenyl ether: products and quantum yield. Environ. Sci. Technol. 38 (15), 4149–4156.

Brame, J., Li, Q.L., Alvarez, P.J.J., 2011. Nanotechnology-enabled water treatment and reuse: emerging opportunities and challenges for developing countries. Trends Food Sci. Technol. 22 (11), 618–624.

Brame, J.A., Hong, S.W., Lee, J., Lee, S.-H., Alvarez, P.J.J., 2013. Photocatalytic pretreatment with food-grade TiO2 increases the bioavailability and bioremediation potential of weathered oil from the Deepwater Horizon oil spill in the Gulf of Mexico. Chemosphere 90 (8), 2315–2319.

Brame, J., Long, M., Mackeyev, Y., Wilson, L.J., Li, Q., Alvarez, P.J.J., 2014a. Trading Oxidation Power for Efficiency: Differential Inhibition of Photo-generated Hydroxyl Radicals versus Singlet Oxygen Water Research.

Brame, J., Fattori, V., Clarke, R., Mackeyev, Y., Wilson, L.J., Li, Q., Alvarez, P.J.J., 2014b. Water disinfection using nanotechnology for safer irrigation: a demonstration project in Swaziland. Environ. Eng. Sci. 16, 1–9.

Buxton, G.V., Greenstock, C.L., Helman, W.P., Ross, A.B., 1988. Critical review of rate constants for reactions of hydrated electrons, hydrogen atoms and hydroxyl radicals (.OH/.O-) in aqueous Solution. J. Phys. Chem. Ref. Data 17 (2), 513–886.

Chong, M.N., Jin, B., Chow, C.W.K., Saint, C., 2010. Recent developments in photocatalytic water treatment technology: a review. Water Res. 44 (10), 2997–3027.

Doll, T.E., Frimmel, F.H., 2005a. Photocatalytic degradation of carbamazepine, clofibric acid and iomeprol with P25 and Hombikat UV100 in the presence of natural organic matter (NOM) and other organic water constituents. Water Res. 39 (2–3), 403–411.

Doll, T.E., Frimmel, F.H., 2005b. Removal of selected persistent organic pollutants by heterogeneous photocatalysis in water. Catal. Today 101 (3–4), 195–202.

El-Morsi, T.M., Budakowski, W.R., Abd-El-Aziz, A.S., Friesen, K.J., 2000. Photocatalytic degradation of 1,10-dichlorodecane in aqueous suspensions of TiO2: a reaction of adsorbed chlorinated alkane with surface hydroxyl radicals. Environ. Sci. Technol. 34 (6), 1018–1022.

Emeline, A.V., Ryabchuk, V., Serpone, N., 2000. Factors affecting the efficiency of a photocatalyzed process in aqueous metal-oxide dispersions - Prospect of distinguishing between two kinetic models. J. Photochem. Photobiol. A Chem. 133 (1–2), 89–97.

Enriquez, R., Pichat, P., 2001. Interactions of humic acid, quinoline, and TiO2 in water in relation to quinoline photocatalytic removal. Langmuir 17 (20), 6132–6137.

Frontistis, Z., Drosou, C., Tyrovola, K., Mantzavinos, D., Fatta-Kassinos, D., Venieri, D., Xekoukoulotakis, N.P., 2012. Experimental and modeling studies of the degradation of estrogen hormones in aqueous TiO2 suspensions under simulated solar radiation. Ind. Eng. Chem. Res. 51 (51), 16552–16563.

Gomez, D.E., de Blanc, P.C., Rixey, W.G., Bedient, P.B., Alvarez, P.J.J., 2008. Modeling benzene plume elongation mechanisms exerted by ethanol using RT3D with a general substrate interaction module. Water Resour. Res. 44 (5), W05405.

Guillard, C., Puzenat, E., Lachheb, H., Houas, A., Herrmann, J.M., 2005. Why inorganic salts decrease the TiO(2) photocatalytic efficiency. Int. J. Photoenergy 7 (1), 1–9.

Haag, W.R., Hoigne, J., 1986. Singlet oxygen in surface waters. 3. Photochemical formation and steady-state concentrations in various types of waters. Environ. Sci. Technol. 20 (4), 341–348.

Hyung, H., Fortner, J.D., Hughes, J.B., Kim, J.-H., 2006. Natural organic matter stabilizes carbon nanotubes in the aqueous phase. Environ. Sci. Technol. 41 (1), 179–184.

Jafry, H.R., Liga, M.V., Li, Q., Barron, A.R., 2010. Simple route to enhanced photocatalytic activity of P25 titanium dioxide nanoparticles by silica addition. Environ. Sci. Technol. 45 (4), 1563–1568.

Kim, H., Kim, W., Mackeyev, Y., Lee, G.-S., Kim, H.-J., Tachikawa, T., Hong, S., Lee, S., Kim, J., Wilson, L.J., Majima, T., Alvarez, P.J.J., Choi, W., Lee, J., 2012. Selective oxidative degradation of organic pollutants by singlet oxygen-mediated photosensitization: tin porphyrin versus C60 aminofullerene systems. Environ. Sci. Technol. 46 (17), 9606–9613.

Klamerth, N., Malato, S., Agüera, A., Fernández-Alba, A., Mailhot, G., 2012. Treatment of municipal wastewater treatment plant effluents with modified photo-fenton as a tertiary treatment for the degradation of micro pollutants and disinfection. Environ. Sci. Technol. 46 (5), 2885–2892.

Klavarioti, M., Mantzavinos, D., Kassinos, D., 2009. Removal of residual pharmaceuticals from aqueous systems by advanced oxidation processes. Environ. Int. 35 (2), 402–417.

Konstantinou, I.K., Albanis, T.A., 2004. TiO2-assisted photocatalytic degradation of azo dyes in aqueous solution: kinetic and mechanistic investigations: a review. Appl. Catal. B Environ. 49 (1), 1–14.

Lee, Y., von Gunten, U., 2010. Oxidative transformation of micropollutants during municipal wastewater treatment: comparison of kinetic aspects of selective (chlorine, chlorine dioxide, ferrateVI, and ozone) and non-selective oxidants (hydroxyl radical). Water Res. 44 (2), 555–566.

Lee, J., Mackeyev, Y., Cho, M., Li, D., Kim, J.-H., Wilson, L.J., Alvarez, P.J.J., 2009. Photochemical and antimicrobial properties of novel C60 derivatives in aqueous systems. Environ. Sci. Technol. 43 (17), 6604–6610.

Lee, J., Mackeyev, Y., Cho, M., Wilson, L.J., Kim, J.-H., Alvarez, P.J.J., 2010. C60 aminofullerene immobilized on silica as a visible-light-activated photocatalyst. Environ. Sci. Technol. 44 (24), 9488–9495.

Lee, J., Hong, S., Mackeyev, Y., Lee, C., Chung, E., Wilson, L.J., Kim, J.-H., Alvarez, P.J.J., 2011. Photosensitized oxidation of emerging organic pollutants by tetrakis C60 aminofullerene-derivatized silica under visible light irradiation. Environ. Sci. Technol. 45 (24), 10598–10604.

Liao, Y., Brame, J., Que, W., Xiu, Z., Xie, H., Li, Q., Fabian, M., Alvarez, P.J., 2013. Photocatalytic generation of multiple ROS types using low-temperature crystallized anodic TiO2 nanotube arrays. J. Hazard. Mater. 260 (0), 434–441.

Martínez, C., Canle, L.M., Fernández, M.I., Santaballa, J.A., Faria, J., 2011. Aqueous degradation of diclofenac by heterogeneous photocatalysis using nanostructured materials. Appl. Catal. B Environ. 107 (1–2), 110–118.

Minero, C., 1999. Kinetic analysis of photoinduced reactions at the water semiconductor interface. Catalysis Today 54, 205–216.

Minero, C., Mariella, G., Maurino, V., Vione, D., Pelizzetti, E., 2000. Photocatalytic transformation of organic compounds in the presence of inorganic ions. 2. Competitive reactions of phenol and alcohols on a titanium Dioxide–Fluoride system. Langmuir 16 (23), 8964–8972.

Qu, X., Brame, J., Li, Q., Alvarez, P.J.J., 2012. Nanotechnology for a safe and sustainable water Supply: enabling integrated water treatment and reuse. Acc. Chem. Res. 46 (3), 834–843.

Saltelli, A., Ratto, M., Tarantola, S., Campolongo, F., 2005. Sensitivity analysis for chemical models. Chem. Rev. 105 (7), 2811–2828.

Skovsen, E., Snyder, J.W., Lambert, J.D.C., Ogilby, P.R., 2005. Lifetime and diffusion of singlet oxygen in a cell. J. Phys. Chem. B 109 (18), 8570–8573.

Tachikawa, T., Majima, T., 2009. Single-molecule fluorescence imaging of TiO2 photocatalytic reactions. Langmuir 25 (14), 7791–7802.

Turchi, C.S., Ollis, D.F., 1990. Photocatalytic degradation of organic water contaminants: mechanisms involving hydroxyl radical attack. J. Catal. 122 (1), 178–192.

Wilkinson, F., Helman, W.P., Ross, A.B., 1995. Rate constants for the decay and reactions of the lowest electronically excited singlet state of molecular oxygen in solution. An expanded and revised compilation. J. Phys. Chem. Ref. Data 24 (2), 663–677.

Zhang, F.L., Zhao, J.C., Shen, T., Hidaka, H., Pelizzetti, E., Serpone, N., 1998. TiO2-assisted photodegradation of dye pollutants - II. Adsorption and degradation kinetics of eosin in TiO2 dispersions under visible light irradiation. Appl. Catal. B Environ. 15 (1–2), 147–156.

Zhang, G.S., Nadagouda, M.N., O'Shea, K., El-Sheikh, S.M., Ismail, A.A., Likodimos, V., Falaras, P., Dionysiou, D.D., 2014. Degradation of cylindrospermopsin by using polymorphic titanium dioxide under UV-Vis irradiation. Catal. Today 224, 49–55.